NASA TECHNICAL MEMORANDUM

NASA TM X-2966

NASA TM X-2966

LOW-SPEED WIND-TUNNEL INVESTIGATION OF THE AERODYNAMIC AND ACOUSTIC PERFORMANCE OF A TRANSLATING-GRID CHOKED-FLOW INLET

by John M. Abbott, Brent A. Miller, and Richard L. Golladay

Lewis Research Center
Cleveland, Ohio 44135

NATIONAL AERONAUTICS AND SPACE ADMINISTRATION • WASHINGTON, D. C. • FEBRUARY 1974

1. Report No.	2. Government Accession No.	3. Recipient's Catalog No.
NASA TM X-2966		

4. Title and Subtitle	5. Report Date
LOW-SPEED WIND-TUNNEL INVESTIGATION OF THE AERODYNAMIC AND ACOUSTIC PERFORMANCE OF A TRANSLATING-GRID CHOKED-FLOW INLET	February 1974
	6. Performing Organization Code

7. Author(s)	8. Performing Organization Report No.
John M. Abbott, Brent A. Miller, and Richard L. Golladay	E-7562
	10. Work Unit No. 501-24

9. Performing Organization Name and Address	11. Contract or Grant No.
Lewis Research Center National Aeronautics and Space Administration Cleveland, Ohio 44135	
	13. Type of Report and Period Covered
12. Sponsoring Agency Name and Address	Technical Memorandum
National Aeronautics and Space Administration Washington, D.C. 20546	14. Sponsoring Agency Code

15. Supplementary Notes

16. Abstract

The aerodynamic and acoustic performance of a translating grid choked-flow inlet was determined in a low-speed wind tunnel at free-stream velocities of 24, 32, and 45 m/sec and incidence angles of 0°, 10°, 20°, 30°, 35°, 40°, 45°, and 50°. The inlet was sized to fit a 13.97-centimeter-diameter fan with a design weight flow of 2.49 kg/sec. Measurements were made to determine inlet total pressure recovery, flow distortion, and sound pressure level for both choked and unchoked geometries over a range of inlet weight flows. For the unchoked geometry, inlet total pressure recovery ranged from 0.983 to 0.989 at incidence angles less than 40°. At 40° incidence angle, inlet cowl separation was encountered which resulted in lower values of pressure recovery and higher levels of fan broadband noise. For the choked geometry, increasing total pressure losses occurred with increasing inlet weight flow that prevented the inlet from reaching full choked conditions with the particular fan used. These losses were attributed to the high Mach number drag rise characteristics of the airfoil grid. At maximum attainable inlet weight flow, the total pressure recovery at static conditions was 0.935. The fan blade passing frequency and other fan generated pure tones were eliminated from the noise spectrum, but the broadband level was increased.

17. Key Words (Suggested by Author(s))	18. Distribution Statement
Inlet design; Sonic inlet; Choked inlet; Acoustic suppression; Pressure recovery; Noise reduction; Wind-tunnel tests	Unclassified - unlimited Cat. 28

19. Security Classif. (of this report)	20. Security Classif. (of this page)	21. No. of Pages	22. Price*
Unclassified	Unclassified	31	$3.00

*For sale by the National Technical Information Service, Springfield, Virginia 22151

LOW-SPEED WIND-TUNNEL INVESTIGATION OF THE AERODYNAMIC AND ACOUSTIC PERFORMANCE OF A TRANSLATING-GRID CHOKED-FLOW INLET

by John M. Abbott, Brent A. Miller, and Richard L. Golladay

Lewis Research Center

SUMMARY

The aerodynamic and acoustic performance of a translating grid choked-flow inlet was determined in a low-speed wind tunnel at free-stream velocities of 24, 32, and 45 meters per second and incidence angles of 0°, 10°, 20°, 30°, 35°, 40°, 45°, and 50°. The inlet was sized to fit a 13.97-centimeter-diameter fan with a design weight flow of 2.49 kilograms per second. Measurements were made to determine inlet total pressure recovery, flow distortion, and sound pressure level for both choked and unchoked geometries over a range of inlet weight flows.

For the unchoked geometry, inlet total pressure recovery ranged from 0.983 to 0.989 at incidence angles less than 40°. At 40° incidence angle, inlet cowl separation was encountered which resulted in lower values of pressure recovery and higher levels of fan broadband noise.

For the choked geometry, increasing total pressure losses occurred with increasing inlet weight flow that prevented the inlet from reaching full choked conditions with the particular fan used. These losses were attributed to the high Mach number drag rise characteristics of the airfoil grid. At maximum attainable inlet weight flow, the total pressure recovery at static conditions was 0.935. The fan blade passing frequency and other fan generated pure tones were eliminated from the noise spectrum, but the broadband level was increased.

INTRODUCTION

Future commercial aircraft presently under study, such as the nearsonic transport, the advanced supersonic transport, and short haul (STOL) aircraft, will all be required

to meet stringent noise specifications. The primary source of aircraft noise is the engine and current designs cannot meet future noise goals without some form of noise suppression. It has been shown that compressor and fan noise radiating from the engine inlet can be reduced by choking the inlet airflow. Experiments have been conducted at static conditions to determine the acoustic and aerodynamic performance of inlets that attained choked flow using inlet guide vanes, contracting cowl walls, radial vanes, a translating centerbody and a translating grid of airfoils (refs. 1 to 4). In reference 5, the performance of a scale model translating centerbody choked flow inlet was presented over a range of free-stream velocities and incidence angles.

The purpose of the present investigation was to measure the effects of free-stream velocity and incidence angle on the aerodynamic and acoustic performance of a translating grid choked flow inlet. This type of inlet is of interest because the use of multiple flow passages may result in a shorter and lighter inlet than that attainable with a single flow passage. The inlet was sized to fit a 13.97-centimeter-diameter fan. Inlet performance was determined in a wind tunnel at free-stream velocities of 24, 32, and 45 meters per second and incidence angles of 0° to 50°. Inlet total pressure recovery, flow distortion, and acoustic performance are presented for the inlet operating in both choked and unchoked geometries.

SYMBOLS

BPF blade passing frequency, Hz

c airfoil chord length, cm

D_{max} inlet total pressure distortion parameter computed using all 48 measured total pressures at rake measuring plane, (maximum total pressure - minimum total pressure)/(average total pressure)

D'_{max} inlet total pressure distortion parameter computed without 8 total pressures measured closest to outer wall at rake measuring plane, (maximum total pressure - minimum total pressure)/(average total pressure)

D_T cowl throat diameter, cm

D_{60} inlet circumferential total pressure distortion parameter, (average total pressure - minimum average total pressure over any 60° circumferential sector)/(average total pressure)

L cowl length, cm

M average throat Mach number computed assuming one-dimensional flow

N fan rotational speed, rpm

P_o free-stream total pressure, N/m^2

P_1 area averaged total pressure at rake measuring plane, N/m^2

$P_{1,l}$ local total pressure at rake measuring plane, N/m^2

p_1 average tip static pressure at rake measuring plane, N/m^2

R_H flow passage hub radius at rake measuring plane, cm

R_T flow passage tip radius at rake measuring plane, cm

V_o free-stream velocity, m/sec

W distance from rake measuring plane to fan rotor, cm

Z distance from airfoil trailing edge to rake measuring plane, cm

α incidence angle; angle between free-stream velocity and inlet centerline, deg

θ fan inlet corrected temperature, (fan inlet temperature in K)/(288.2 K)

ψ inlet circumferential position, deg

APPARATUS AND PROCEDURE

Shown in figure 1 is a general layout of the test installation in the Lewis Research Center 9- by 15-Foot V/STOL Wind Tunnel (ref. 6). The model was mounted on a turntable for testing at various incidence angles. Microphones were mounted upstream of the test section in the tunnel settling chamber to measure inlet radiated fan noise.

The test model consisted of a test inlet, a fan, exhaust ducting, and an exhaust noise muffler. The single-stage, 13.97-centimeter-diameter, tip turbine driven fan was used both as a suction source and noise generator. The fan has 16 rotor blades resulting in a blade passing frequency of 9600 hertz at the fan design speed of 36 000 rpm. Design pressure ratio is 1.25 at a weight flow of 2.49 kilograms per second. More details of the fan performance are given in reference 7.

The inlets were mounted to the fan by use of an adapter section containing the supports for the stationary centerbody as well as the total pressure rakes used to measure inlet performance (see fig. 2).

Inlet Design

As shown in figure 2, the translating grid inlet attains choked flow by a translation of the downstream airfoil grid section into the plane of the upstream grid section. This forms eight separate choked-flow passages that distinguish this inlet from the single

choked-flow passage inlet described in reference 5. The translating grid inlet may result in a reduction in inlet length and weight as a result of the shorter diffusion length attainable with multiple flow passages.

Translating grid inlet in unchoked geometry. - Shown in figure 2(a) is the translating grid inlet in the unchoked geometry. The airfoil grids are separated as they would be during cruise operation where inlet choking for noise suppression is not required. The seven airfoils are of equal thickness and were uniformly spaced across the inlet duct. The airfoil sections used have the NACA 65_2-015 basic thickness shape with a chord of 3.48 centimeters and a maximum thickness of 0.523 centimeter. The trailing edge of the downstream airfoils is approximately 1.5 chord lengths ahead of the rake measuring plane. Two side fairings or fillets were used to reduce losses near the duct wall.

The design grid throat Mach number is 0.59 through the four downstream airfoils at the design weight flow of 2.49 kilograms per second. The grid throat Mach number through the three upstream airfoils is approximately the same, 0.58. More details of the design axial Mach number distribution through the airfoils are given in reference 4.

The external cowl has a NACA series 1 shape with an external diameter ratio (highlight diameter/maximum diameter) of 0.865 and a drag rise Mach number of approximately 0.80. The cowl internal lip is a two-to-one ellipse. The contraction ratio (highlight area/throat area) is 1.30. The spinner is a NACA series 1 design with a length-to-diameter ratio of one. Further details of the cowl and spinner design are also given in reference 4.

Translating grid inlet in choked geometry. - Shown in figure 2(b) is the translating grid inlet in the choked geometry. The four downstream airfoils have been moved forward into the plane of the three stationary upstream airfoils and the minimum flow area occurs at the airfoil maximum thickness plane. This reduces the area through the grid by 16.68 percent resulting in choked flow at the design weight flow of 2.49 kilograms per second. In this position, the airfoils are now approximately 2.3 chord lengths ahead of the rake measuring plane. Details of the axial Mach number distribution through the airfoils are given in reference 4.

Instrumentation and Data Reduction

Test instrumentation gave measurements of inlet pressure recovery and steady-state total pressure distortion at a rake measuring plane located upstream of the actual fan face. This measuring plane is representative of a rotor inlet location. Inlet surface static pressures and inlet radiated noise levels were also measured. No measurements were taken downstream of the fan. Detailed schematics of the instrumentation are given in reference 4.

Rake measuring plane. - As shown in figure 2(b), eight radial total pressure rakes were located in the adapter section at the rake measuring plane. The rakes were spaced each 45° with six total pressure tubes on each rake located at the centroid of equal flow areas. Seven static pressure taps were located on the outer wall of the flow passage between the total pressure rakes.

Inlet cowl. - The inlet cowl was instrumented to measure surface static pressures as shown in figure 2(b). Eleven static pressure taps were located in a row at the $\psi = 0^{\circ}$, or windward, circumferential position. Five of these taps were located on the inlet lip between the highlight and throat and the remaining six were located in the diffuser. An additional five static pressure taps, spaced every 60°, were located in the cowl throat.

Noise measurements. - Noise data were taken with four 0.64-centimeter-diameter microphones located in the wind tunnel settling chamber upstream of the test section. Wind screens were placed on the microphones to minimize wind tunnel flow noise. The hard walls of the wind tunnel approximate a reverberant chamber eliminating any directional noise variation due to changing incidence angle. The four microphone outputs were recorded on magnetic tape, and one channel was selected for processing with a narrow band analyzer. The fan exhaust was ducted out of the test section and into a noise muffler to permit an examination of only the noise being transmitted through the inlet.

Test Procedure

An initial static calibration test was conducted with a bellmouth replacing the inlet cowl. The weight flow measured by the instrumentation at the rake measuring plane was then corrected to agree with the measured bellmouth weight flow. This correction was then applied at the appropriate fan speeds in all the data runs with the inlet cowl in place.

The tests were conducted at free-stream velocities of 0, 24, 32, and 45 meters per second, and at fan corrected speeds from 31 310 to 36 760 rpm. Incidence angles of 0°, 10°, 20°, 30°, 35°, 40°, 45°, and 50° were investigated. The test procedure consisted of setting free-stream velocity, fan corrected speed, and then varying incidence angle from 0° to 50°. The fan corrected speed was then changed and the variation in incidence angle repeated. After taking data at each of the fan corrected speeds, the free-stream velocity was changed. The procedure was then repeated.

RESULTS AND DISCUSSION

Inlet performance is presented in two major parts. The performance of the unchoked inlet geometry (airfoil grids separated, fig. 2(a)) is presented in the first part. The inlet remains unchoked at all fan operating conditions while in this configuration. Presented in the second part is the performance obtained with the choked inlet geometry (downstream airfoil grid moved forward, fig. 2(b)). In this configuration the inlet was designed to operate choked at the fan design speed and unchoked at lower fan speeds.

Unchoked Geometry

Inlet total pressure recovery. - Inlet total pressure recovery is shown in figure 3 as a function of grid throat average Mach number computed at the plane of maximum thickness of the upstream airfoils (minimum grid flow area). The inlet weight flow computed from the total and static pressure measurements at the rake measuring plane was used to determine this Mach number. Total pressure recovery is based on the area averaged total pressure at the rake measuring plane.

As shown in figure 3(a), some scatter was measured in inlet total pressure recovery at static conditions. However, a general trend can be detected that indicates a decrease in total pressure recovery from 0.989 to 0.985 as grid throat average Mach number increases from 0.50 to 0.60. With the airfoil grid section removed, the data of reference 5 show a pressure recovery of between 0.996 and 0.998 as shown by the dashed line on the figure. The lower total pressure recovery for the grid inlet is attributed to losses through the airfoils.

Total pressure recovery at a free-stream velocity of 24 meters per second and incidence angles of 0°, 20°, 40°, and 50° is presented in figure 3(b). The slight irregularity in total pressure recovery shown at static conditions is no longer present due to improved cowl lip performance with free-stream velocity. Increasing grid throat Mach number at all incidence angles reduced pressure recovery. At 0° incidence angle, the total pressure recovery is reduced from 0.987 to 0.984, as the grid throat Mach number increases from 0.523 to 0.601, about the same as observed at static conditions. An increase in incidence angle above 40° also produced a small reduction in recovery. At a grid throat Mach number of 0.56, the pressure recovery is reduced from 0.985 to 0.984 while increasing incidence angle from 40° to 50°. Changing incidence angle below 40° had little effect on recovery.

Shown in figure 3(c) is the effect of increasing the free-stream velocity to 32 meters per second. At incidence angles from 0° to 40°, the results are similar to those shown at a free-stream velocity of 24 meters per second. However, as incidence angle was

increased from 40° to 50° there was an abrupt drop in recovery of about 2 percent over the entire range of grid throat Mach numbers. Examination of the axial variation of the cowl surface static pressure indicated flow separation had occurred on the inlet cowl lower lip in the same manner as reported in reference 5 for the inlet without the airfoil grids. The effect of this separation on total pressure distortion and acoustic performance will be discussed later.

A further increase in free-stream velocity to 45 meters per second, resulted in the total pressure recoveries shown in figure 3(d). At this free-stream velocity, flow separation occurred on the cowl lip at an incidence angle of 40°, with a consequent drop in recovery of about 2 percent. At incidence angles below 40°, the results are similar to those shown at lower free-stream velocities.

Several data points in figure 3(d) are labeled by the letters, A, B, and C for convenience in identifying these same points in several figures that follow.

Summarizing, the data of figure 3 indicate that for incidence angles where flow separation on the cowl lip was not encountered, increasing grid throat Mach number or increasing incidence angle resulted in only small decreases in inlet total pressure recovery. Recoveries ranged from 0.989 to 0.983 with the lower value occurring at high grid throat Mach number and high incidence angle. Flow separation on the cowl lip was encountered at 50° incidence angle at a free-stream velocity of 32 meters per second, and at 40° incidence angle at a 45-meter-per-second free-stream velocity. Both of these conditions resulted in a 2 percent drop in recovery.

Total pressure distribution and distortion. - The distribution of total pressure at the rake measuring plane is shown in figure 4 for the points labeled A, B, and C on figure 3(d). The local total pressure ratio is shown at each probe location in the rake measuring plane.

Presented in figure 4(a) is the total pressure distribution measured at 0° incidence angle (data point A). The free-stream velocity is 45 meters per second and the total pressure recovery is 0.986. As expected, lower total pressures were generally observed on these total pressure probes located behind the airfoil sections. This is particularly evident for the total pressure rakes located horizontally on the figure. Low total pressures were also measured by the probes located closest to the outer wall. This is a result of boundary layer losses and the losses generated in the corners where the airfoil sections intersect the outer wall.

Increasing incidence angle to 30° (data point B) resulted in the total pressure distribution shown in figure 4(b). Total pressure recovery is the same as data point A (0.986) and the total pressure distribution is nearly the same as that shown at 0° incidence angle. The result of increasing incidence angle to 40° is presented in figure 4(c) (data point C) where flow separation occurred on the inlet cowl. A low total pressure region is shown in the lower portion of the figure centered about the $\psi = 0^{\circ}$ or lower lip

of the inlet. The total pressure distribution in the upper half of the inlet remained relatively unchanged. The total pressure recovery dropped to 0.964.

Total pressure distortion measured at the rake measuring plane is shown in figure 5 as a function of grid throat average Mach number. Presented in figure 5(a) are the distortions measured at static conditions. Three distortion parameters, D_{max}, D'_{max}, and D_{60}, are shown and are defined in the symbol list. D_{max} is a measure of the minimum total pressure at the rake measuring plane and is computed using all 48 total pressure measurements obtained with the rake. D'_{max} is determined in the same manner as D_{max}, however, the eight total pressure measurements made closest to the outer wall are not included in the calculation. Thus, the low total pressures measured near the outer wall (fig. 4) due to boundary layer and corner losses, are not included in the computation of D'_{max}. D_{60} indicates the presence of a circumferential variation in the total pressure.

As shown in figure 5(a), at static conditions D_{max} varies between 0.052 and 0.090 over the grid throat Mach number range from 0.487 to 0.600. Over this same range of operating conditions D'_{max} varies between 0.022 and 0.031. As already mentioned, the difference between D_{max} and D'_{max} is due to the total pressure losses measured near the outer wall. D_{60} is always less than 0.009 indicating little circumferential distortion.

At a free-stream velocity of 24 meters per second, figure 5(b), increasing grid throat average Mach number is shown to result in increasing values of D_{max}. At an incidence angle of zero degrees, D_{max} increases from 0.062 to 0.082 as grid throat Mach number increases from 0.523 to 0.601. D_{max} also tended to increase slightly as incidence angle was increased. Values of D'_{max} are not shown in the figure, however, the relation between D'_{max} and D_{max} is the same as that indicated at static conditions. D_{60} is less than 0.005 over the range of grid throat average Mach number which again indicates little circumferential distortion.

Shown in figure 5(c) are the same effects of incidence angle and grid throat Mach number on total pressure distortions at a free-stream velocity of 32 meters per second. However, when flow separation occurred on the inlet cowl at an incidence angle of 50°, D_{max}, D'_{max}, and D_{60} increased substantially reflecting the decrease in total pressure recovery shown in figure 3(c).

At a free-stream velocity of 45 meters per second, figure 5(d), the total pressure distortions again reflect the occurrence of flow separation on the inlet cowl at 40° incidence angle. At lower incidence angles, increasing grid throat Mach number and incidence angle affected the total pressure distortion as discussed previously.

Summarizing, figures 4 and 5 indicate that for incidence angles where flow separation on the cowl lip was not encountered, increasing grid throat Mach number or increasing incidence angle results in an increase in the distortion parameter D_{max}.

D'_{max} was less than D_{max} reflecting the presence of boundary layer and corner losses near the outer wall of the inlet. D_{60} remained unaffected over these operating conditions, suggesting little circumferential distortion. At incidence angles below 40^{o}, D_{max} remained below 0.075, D'_{max} below 0.032, and D_{60} below 0.010. Flow separation on the cowl lip at incidence angles of 40^{o} and 50^{o} produced large increases in the three distortion parameters.

Acoustic performance. - The effect of incidence angle on the narrow band noise spectrum of the inlet radiated fan noise is shown in figure 6 for a free-stream velocity of 45 meters per second. Changing incidence angle from 0^{o} to 30^{o} had no systematic effect on fan noise generation. The change in measured noise at these incidence angles is shown by the cross-hatched band in the figure. However, at 40^{o} incidence angle (data point C), where flow separation on the inlet cowl occurred, the broadband noise generation of the fan increased greatly due to the distorted inflow. Note the decrease in sound pressure level at the fan blade passing frequency (BPF) with inlet cowl flow separation. This may be due to a disturbance of the fan blade passing noise generation mechanism caused by the distorted inflow.

It should be remembered that for this particular installation, the fan was located some distance downstream of the rake measuring plane, suggesting lower values of distortion at the fan than those measured by the rakes. Had the fan been located at the rake measuring plane, inlet flow distortions may have produced different acoustic results, perhaps a greater broadband noise increase.

Choked Geometry

In the discussion of the unchoked geometry, performance was presented as a function of the grid throat average Mach number computed from the measured inlet weight flow. Values of Mach number were no greater than 0.62. This method of data presentation is satisfactory as long as the Mach number does not exceed approximately 0.70. Above this value, any errors in determining inlet weight flow produce progressively larger errors in the computed Mach number. Errors in the weight flow measurement may result from the presence of airfoil wakes at the rake measuring plane or uncertainties as to what the actual grid throat flow area is. For these reasons, grid throat average Mach number was not used as a correlating parameter for presenting data with the inlet in the choked geometry. Instead, data are presented as a function of the ratio of the average static pressure measured on the outer wall at the rake measuring plane to the free stream total pressure. This pressure ratio indicates the degree of suction applied to the inlet and was found to be useful for presenting inlet performance. Grid throat average Mach number computed from the inlet weight flow is also presented,

however, to indicate the general level of that parameter.

Inlet total pressure recovery and grid throat average Mach number. - Presented in figure 7 are inlet total pressure recovery and grid throat average Mach number as a function of rake plane pressure ratio. In addition, shown in figure 7(a) is the relation between cowl throat surface static pressure to free-stream total pressure ratio and rake plane pressure ratio at static conditions. The effect of increasing inlet suction (increasing fan speed) can be seen by moving toward the left side of the figure to lower values of rake plane pressure ratio. Movement in this direction initially increases the grid throat average Mach number and decreases cowl throat surface static pressure, reflecting an increase in inlet weight flow. Total pressure recovery decreases.

As the rake plane static pressure ratio is further reduced, grid throat Mach number and cowl throat surface static pressure ratio tend to flatten out while the total pressure recovery begins to decrease at a faster rate. This region of constant grid throat Mach number and cowl throat surface static pressure (constant inlet weight flow) may at first be interpreted as a result of attaining choked flow. However, increasing inlet suction to a value of rake plane pressure ratio of 0.74 results in a further increase in grid throat Mach number and a decrease in cowl throat surface static pressure indicating an increase in inlet weight flow. Had the inlet flow been choked, the weight flow could again increase only if the choked flow throat area increased or the total pressure in the throat increased. Both of these explanations are unlikely. Instead, the results indicate that the region of constant grid throat Mach number and cowl throat surface static pressure was not due to attaining choked flow but a result of the rapid decrease in total pressure recovery over the range of rake plane static pressure ratio from 0.74 to 0.79. Increasing fan speed results in a larger total pressure rise across the fan, however, combined with the rapid decrease in inlet total pressure recovery, there is no net increase in inlet weight flow.

The rapid decrease in inlet total pressure recovery shown in figure 7(a) is attributed to reaching the drag divergence Mach number of the airfoil section. The critical Mach number for the isolated airfoil section used in this investigation at 0° incidence angle is 0.72 (ref. 8). In the drag rise operating region, increasing inlet suction produces a large increase in drag on the airfoils resulting in the corresponding rapid decrease in total pressure recovery shown in figure 7(a). At a rake plane pressure ratio of approximately 0.74, sufficient inlet suction was applied to pass beyond the drag rise region and result in a slower decrease in inlet total pressure recovery. The increase in pressure rise across the fan due to increasing fan speed now dominates over the slower rate of decreasing inlet pressure recovery and the grid throat Mach number again increases and the cowl throat surface static pressure again decreases.

At the design rotational speed of the fan (36 000 rpm), the rake plane pressure ratio was 0.733 with a total pressure recovery of 0.936. At this fan speed and at the maximum attainable overspeed value (rake plane pressure ratio of 0.725, pressure recovery

of 0.935), sufficient suction could not be applied to the inlet to overcome the inlet total pressure losses and attain fully choked flow through the grid section with the particular fan used. An examination of the acoustic data will show this same result.

Data obtained at a free-stream velocity of 24 meters per second and incidence angles of 0°, 20°, 40°, and 50° are shown in figure 7(b). The lines on the figure are curve fits to the static data of figure 7(a). The data points indicate little or no effect of incidence angle on total pressure recovery. Over the range of operating conditions presented, however, the pressure recovery is higher because of the improved cowl lip performance due to operating with free-stream velocity. At a rake plane pressure ratio of 0.80, the pressure recovery increased from an average value of 0.971 to 0.977 as free-stream velocity increased from 0 to 24 meters per second.

The effect of increasing the free-stream velocity to 32 meters per second is shown in figure 7(c). Little or no effect of incidence angle is indicated until an angle of 45° is reached where flow separation on the inlet cowl occurred. The data at incidence angles below 45° show the same trend as the static data. Free-stream velocity has again resulted in an increase in the total pressure recovery over the range of operating conditions. One data point in the figure shows a computed grid throat Mach number of 1.0. An examination of the acoustic data, however, showed no signs of inlet noise suppression suggesting that the computed Mach number may be imprecise for the reasons previously discussed.

At a free-stream velocity of 45 meters per second, figure 7(d), the same effects of incidence angle and free-stream velocity on inlet performance are shown. Flow separation at 40° incidence angle resulted in lower pressure recoveries and lower grid throat Mach numbers. Another data point was found to have a computed grid throat Mach number of 1.0, however, again the acoustic data indicated little inlet noise suppression suggesting some imprecision in the Mach number computation. Several data points are labeled on figure 7(d) with the letters D, E, F, and G for convenience in identifying these points on subsequent figures.

Summarizing figure 7, total pressure losses were encountered while operating with the choked geometry that prevented the inlet from reaching a full choke condition with the particular fan used. These losses are attributed to the high Mach number drag rise characteristics of the airfoil grid. With the maximum attainable inlet weight flow, the total pressure recovery at static conditions was 0.935 with a grid throat average Mach number of 0.945. Free-stream velocity improved the inlet total pressure recovery when the flow on the cowl lip was not separated. Incidence angle had little or no effect on pressure recovery until flow separation occurred. As shown for the unchoked geometry, inlet lip flow separation occurred at lower incidence angles at higher free-stream velocities. Rake plane static to free-stream total pressure ratio was a convenient parameter for defining inlet operating conditions.

The aerodynamic results discussed in this section may have been significantly different had the airfoil grid sections been designed with a different thickness-to-chord ratio. The drag rise characteristics of an airfoil section are dependent on the thickness-to-chord ratio. The airfoil grid sections used in this investigation had a thickness-to-chord ratio of 0.15. A reduction in this ratio would result in a delay in the onset of drag rise and a greater value of grid throat Mach number could be attained before large drag rise losses were encountered. Decreasing the thickness-to-chord ratio, however, would result in either a larger number of thinner airfoils or airfoils with a longer chord length. Any additional losses that result from these changes would require consideration in determining any net gain due to a reduction in the airfoil thickness-to-chord ratio.

Total pressure distribution and distortion. - The total pressure distributions measured at the rake measuring plane are shown in figure 8 for the points labeled D, E, F, and G on figure 7(d). Shown in figure 8(a), data point D, is the total pressure distribution measured at 0° incidence angle and a rake plane pressure ratio of 0.822. Free-stream velocity is 45 meters per second and total pressure recovery is 0.979. The effect of decreasing rake plane pressure ratio on the total pressure distribution can be seen in figure 8(b), data point E. Rake plane pressure ratio has decreased to 0.728 and pressure recovery has decreased to 0.942. The decrease in total pressure is uniform over the rake measuring plane. Shown in figure 8(c) is the effect of increasing incidence angle to 35°. Rake plane pressure ratio is 0.739 and pressure recovery is 0.943. This increase in incidence angle shows little effect on the total pressure distribution. In figure 8(d) the effect of inlet cowl flow separation on total pressure distribution can be seen. The incidence angle is 40° (data point G) and the pressure recovery has dropped to 0.924. Note the low values of total pressure ratio centered about the $\psi = 0^{\circ}$ or windward portion of the inlet.

Shown in figure 9 is the total pressure distortion encountered while operating with the choked geometry. At static conditions (fig. 9(a)), D_{max} varies from 0.045 to 0.120 and D'_{max} varies from 0.034 to 0.113 with D_{max} being greater than D'_{max} for any given data point. Values of D_{60} remain below 0.027 over the range of operating conditions.

Shown in figure 9(b) is the effect of incidence angle on total pressure distortion at a free-stream velocity of 24 meters per second. D_{max} remained below 0.080 at all conditions. Values of D'_{max} are not shown in the figure, however, the relation between D'_{max} and D_{max} is the same as that indicated at static conditions. D_{60} remained below 0.010 and was not affected by incidence angles up to 50°. At 32 meters per second (fig. 9(c)), the flow separation on the inlet cowl encountered at 45° incidence angle resulted in larger values of D_{max}, D'_{max}, and D_{60}. At lower incidence angles, no consistent effect of incidence angle occurred over the range of rake plane pressure ratio.

At all incidence angles, decreasing the rake plane pressure ratio resulted in higher values of D_{max} and D_{60}.

Shown in figure 9(d) are the results of further increasing the free-stream velocity to 45 meters per second. The same effects of incidence angle and rake plane pressure ratio are shown. At 0^{o} incidence angle, decreasing rake plane pressure ratio from 0.822 to 0.727 (data point D to E) produced an increase in D_{max} and D_{60} from 0.063 to 0.131 and from 0.007 to 0.036, respectively. Increasing incidence angle had no consistent effect on distortion until flow separation occurred at an incidence angle of 40^{o}. As incidence angle was increased from 35^{o} to 40^{o} (data point F to G), D_{max} and D_{60} increased from 0.097 to 0.170 and 0.014 to 0.017, respectively.

Summarizing, figures 8 and 9 indicate that, for incidence angles where flow separation was not encountered, decreasing rake plane pressure ratio (increasing grid throat Mach number) increases D_{max}, D'_{max}, and D_{60}. Increasing incidence angle had no consistent effect on distortion until inlet cowl flow separation was encountered. This resulted in significantly higher values of D_{max}, D'_{max}, and D_{60}.

Acoustic performance. - Presented in figure 10 is a comparison of the narrow band noise spectra for the choked and unchoked geometries at a free-stream velocity of 45 meters per second and 0^{o} incidence angle (data points A and E). Maximum inlet suction (minimum rake plane pressure ratio) was applied for both points. Also shown in the figure is the narrow band spectrum for the wind tunnel operating alone without the fan. The figure shows the broadband level of the spectrum is higher for the choked inlet geometry than in the unchoked geometry. This effect may be the result of the higher total pressure distortion encountered when operating with the choked geometry. D_{max} has increased from 0.071 to 0.131 and D_{60} from 0.0045 to 0.0363 in changing from the unchoked to the choked geometry. Recall that an increase in broadband noise was shown in figure 6 as a consequence of increasing incidence angle and thus total pressure distortion for the unchoked geometry. Similar results were also presented in reference 5. Note, however, that the fan blade passing frequency (BPF) and the other fan generated pure tones are no longer present with the choked inlet geometry. This may be the result of some inlet suppression due to the high grid throat Mach number or to a disturbance of the fan noise generation mechanism caused by the distorted inflow. Similar results due to incidence angle induced total pressure distortion were shown in figure 6 of this report and reference 5.

As reported in reference 4, the increased noise level encountered for the choked geometry may be partly a result of airfoil flutter. This would account for some of the peaks that occur in the narrow band spectrum at frequencies below 4000 hertz (fig. 10). The general increase in the broadband level, however, is more likely generated by the fan as a result of the distorted inflow.

Shown in figure 11 is the effect of incidence angle on inlet noise generation. For the choked geometry, increasing incidence angle had little effect on the fan narrow band noise spectrum. All the data fell within the cross-hatched band shown in the figure.

In the discussion of figure 6, it was shown that for the unchoked geometry inlet cowl flow separation produced an increase in the fan broadband noise level. Figure 11, however, indicates little or no change in the spectrum when inlet cowl flow separation occurred at an incidence angle of 40° for the choked geometry. This may be a result of the higher distortion levels encountered with the choked operating geometry that may have already generated the high broadband noise levels at lower incidence angles as discussed for figure 10. Thus, little or no change in the narrow band spectrum is indicated when inlet cowl flow separation occurred at 40° incidence angle.

The noise data presented for both the choked and unchoked inlet geometries indicates that fan generated noise is dependent on inlet flow distortion. For the unchoked geometry, cowl flow separation at high incidence angles produced an increase in the fan broadband noise level (fig. 6). The higher distortion levels encountered in the choked operating geometry affected the fan noise generation in the same manner (figs. 10 and 11). Increasing inlet weight flow sufficiently to fully choke the inlet would likely suppress the inlet radiated fan noise. The fan exit noise, however, may still reflect the higher broadband noise level produced by the inlet distortion. This change in fan exit noise characteristics due to inlet produced flow distortions would require consideration in the design of fan exit noise suppression devices.

The acoustic results presented in this report may have been significantly different had the airfoil sections been designed with a different thickness-to-chord ratio. For throat Mach numbers less than the drag divergence value, decreasing the airfoil thickness-to-chord ratio may result in total pressure losses that are somewhat higher due to an increased number of thinner airfoils or airfoils with a longer chord length. The onset of the large drag rise total pressure losses, however, would be delayed to a higher value of throat Mach number. This would directly affect the acoustic results since the amount of inlet noise suppression for a choked-flow inlet has been shown to be dependent on the inlet throat Mach number (refs. 3 to 5). The drag rise Mach number for a finer airfoil section may be sufficiently high to permit inlet noise suppression to be attained before large drag rise total pressure losses and distortions are encountered.

SUMMARY OF RESULTS

The aerodynamic and acoustic performance of a translating grid choked-flow inlet was determined in a low-speed wind tunnel over a range of free-stream velocities and incidence angles with the following results:

1. For the unchoked geometry, inlet total pressure recovery ranged from 0.983 to 0.989 at incidence angles less than 40° with higher values of both grid throat Mach number and incidence angle producing the lower recoveries. Total pressure distortion D_{max} remained below 0.075 over the same range of operating conditions. At 40° incidence angle and a free-stream velocity of 45 meters per second, flow separation on the inlet cowl was encountered, resulting in lower recoveries and higher distortions.

2. For the unchoked geometry, little effect of incidence angle was indicated on inlet acoustic performance for incidence angles where separation on the cowl lip did not occur. At incidence angles where cowl flow separation did occur, however, the broadband noise generation of the fan greatly increased.

3. For the choked geometry, total pressure losses were encountered with increasing inlet weight flow that prevented the inlet from reaching full choked conditions with the particular fan used. With the maximum attainable inlet weight flow, the total pressure recovery at static conditions was 0.935. Increasing inlet weight flow also resulted in higher values of distortion (D_{max}) up to 0.131. An increase in free-stream velocity improved the recovery over all operating conditions, while increases in incidence angle had little or no effect on recovery or distortion until flow separation occurred on the inlet cowl.

4. For the choked geometry, inlet radiated fan noise was not fully suppressed. The fan blade passing frequency and other fan generated pure tones were eliminated from the spectrum, but the broadband spectrum level was increased. This appeared to be the result of increased flow distortion and was found to be independent of incidence angle. Such changes in fan generated noise must be considered in any design of acoustic suppression to reduce fan exit noise with this choked-inlet geometry design concept.

Lewis Research Center,
National Aeronautics and Space Administration,
Cleveland, Ohio, August 20, 1973,
501-24.

REFERENCES

1. Chestnutt, David: Noise Reduction by Means of Inlet-Guide-Vane Choking in an Axial-Flow Compressor. NASA TN D-4682, 1968.

2. Anon.: Study and Development of Turbofan Nacelle Modifications to Minimize Fan-Compressor Noise Radiation. Volume V - Sonic Inlet Development. NASA CR-1715, 1971.

3. Klujber, F.: Results of an Experimental Program for the Development of Sonic Inlets for Turbofan Engines. Paper 73-222, AIAA, Jan. 1973.

4. Miller, Brent A.; and Abbott, John M.: Aerodynamic and Acoustic Performance of Two Choked-Flow Inlets Under Static Conditions. NASA TM X-2629, 1972.

5. Miller, Brent A.; and Abbott, John M.: Low-Speed Wind-Tunnel Investigation of the Aerodynamic and Acoustic Performance of a Translating-Centerbody Choked-Flow Inlet. NASA TM X-2773, 1973.

6. Yuska, Joseph A.; Diedrich, James H.; and Clough, Nestor: Lewis 9- by 15-Foot V/STOL Wind Tunnel. NASA TM X-2305, 1971.

7. Anon.: Installation and Performance Data, Model TD-652 5.5 Inch Tip Turbine Fan. Tech. Development Inc., Aug. 1969.

8. Abbott, Ira H.; von Doenhoff, Albert E.; and Stivers, Louis S., Jr.: Summary of Airfoil Data. NACA TR 824, 1945.

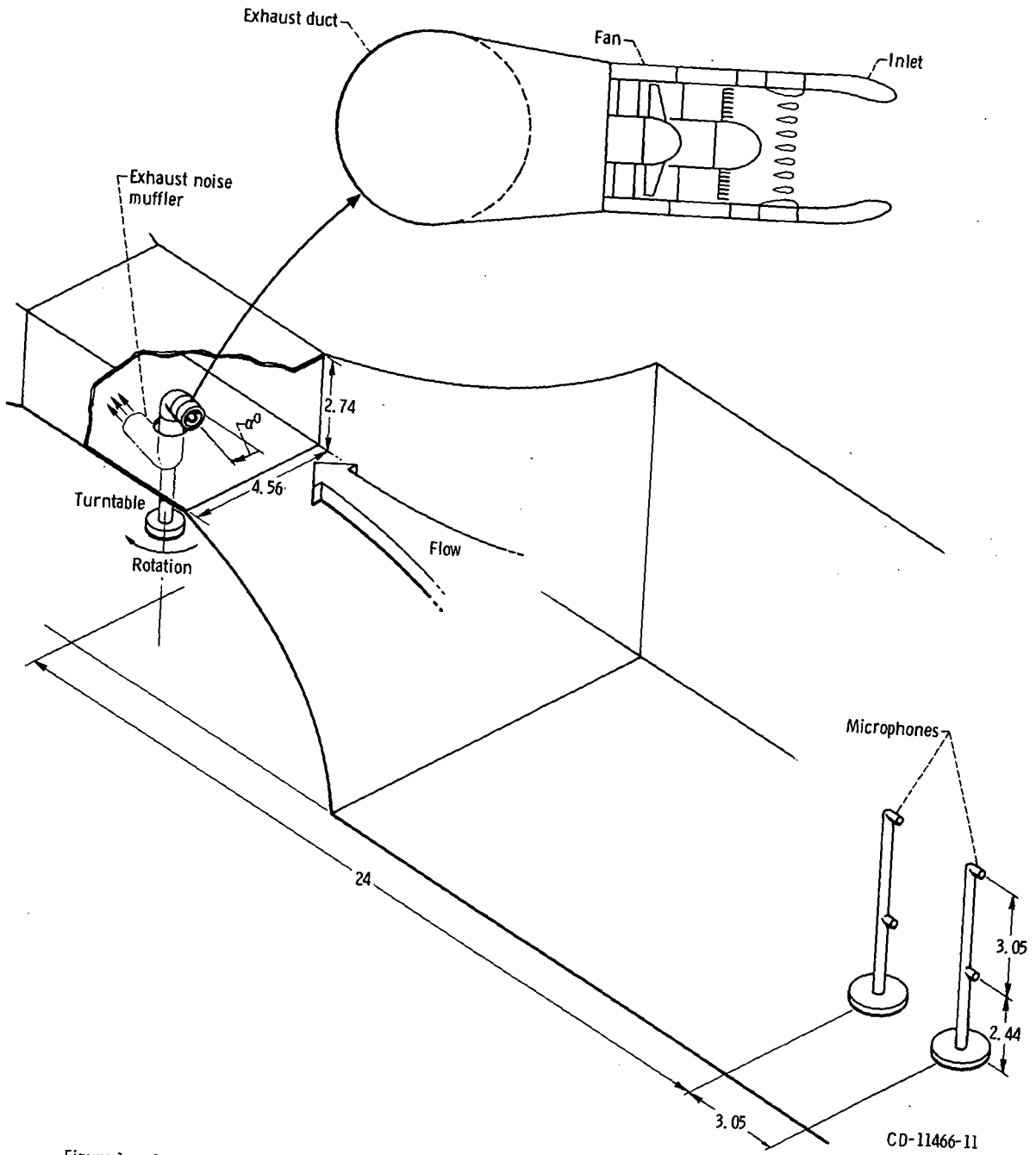

Figure 1. - Schematic view of V/STOL wind tunnel showing model and microphone locations. (All dimensions in m.)

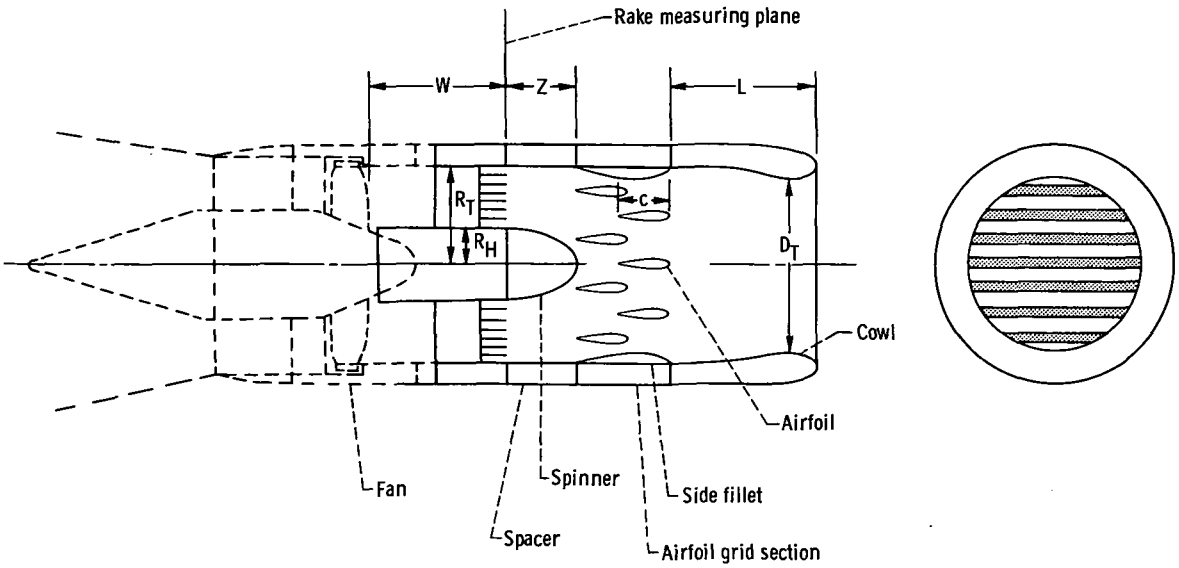

(a) Unchoked geometry (airfoil grids separated). Cowl throat diameter, D_T, 12.55 centimeters; cowl length, L, 10.24 centimeters; airfoil chord length, c, 3.48 centimeters; airfoil thickness to chord ratio, 0.15; distance from airfoil trailing edge to rake measuring plane, Z, 5.08 centimeters; flow passage tip radius at rake measuring plane, R_T, 6.99 centimeters; flow passage hub to tip radius ratio, R_H/R_T, 0.364; distance from rake measuring plane to fan rotor, W, 9.5 centimeters.

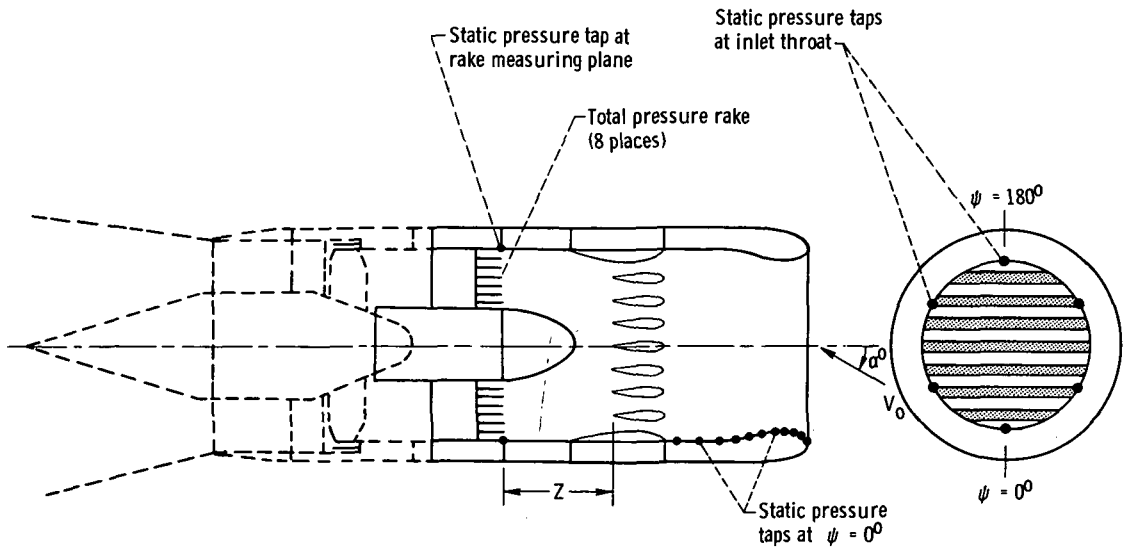

(b) Choked geometry (downstream airfoil grid moved forward). Distance from airfoil trailing edge to rake measuring plane, Z, 7.95 centimeters.

Figure 2. - Schematic view of translating grid inlet.

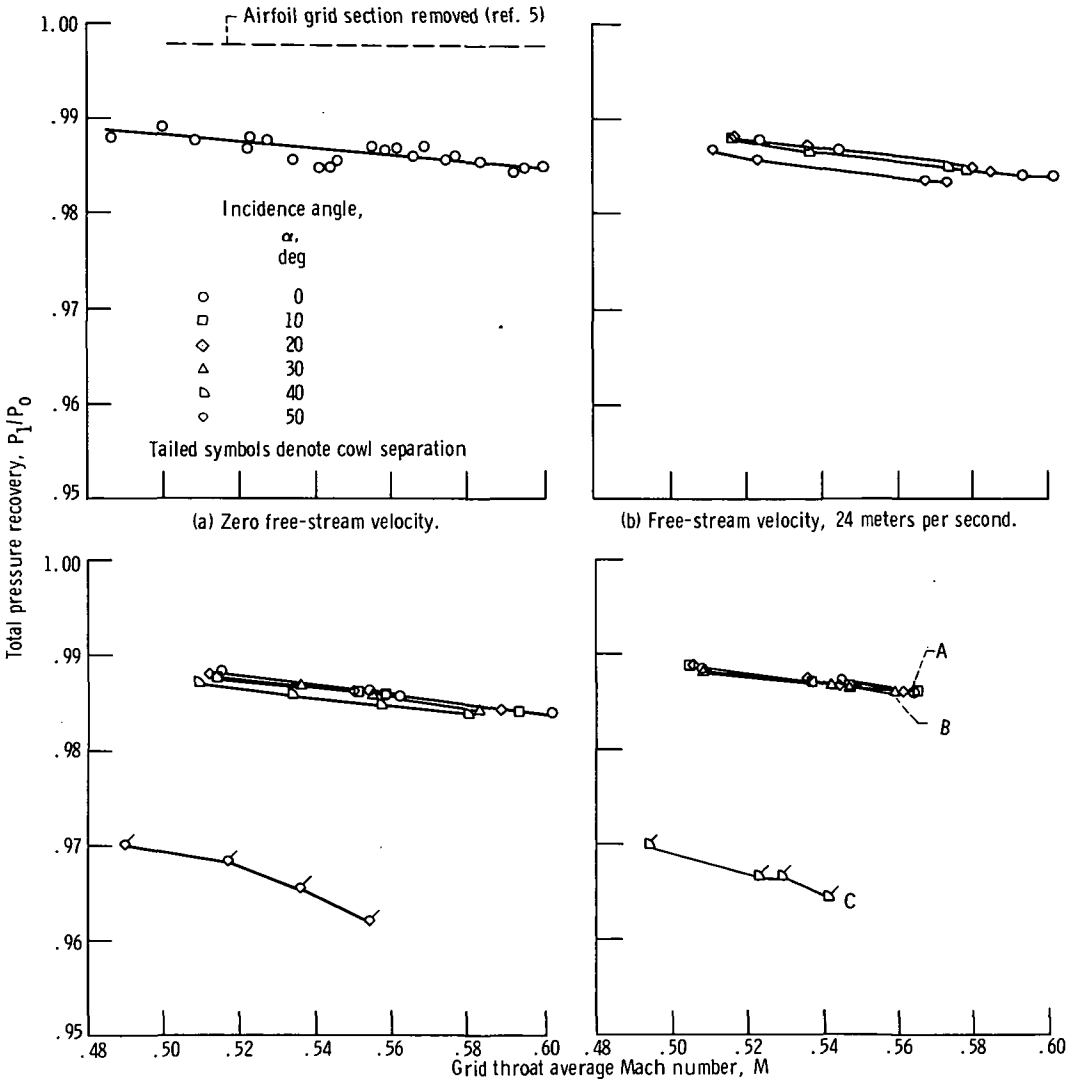

(a) Zero free-stream velocity.

(b) Free-stream velocity, 24 meters per second.

(c) Free-stream velocity, 32 meters per second.

(d) Free-stream velocity, 45 meters per second.

Figure 3. - Total pressure recovery of translating grid inlet in unchoked geometry.

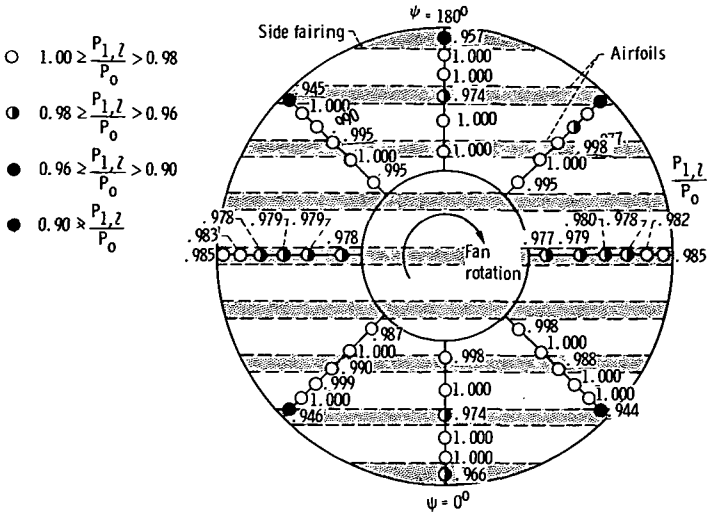

(a) Data point A; incidence angle, 0^0; corrected fan speed, 36 410 rpm; grid throat average Mach number, 0.564; total pressure recovery, 0.986.

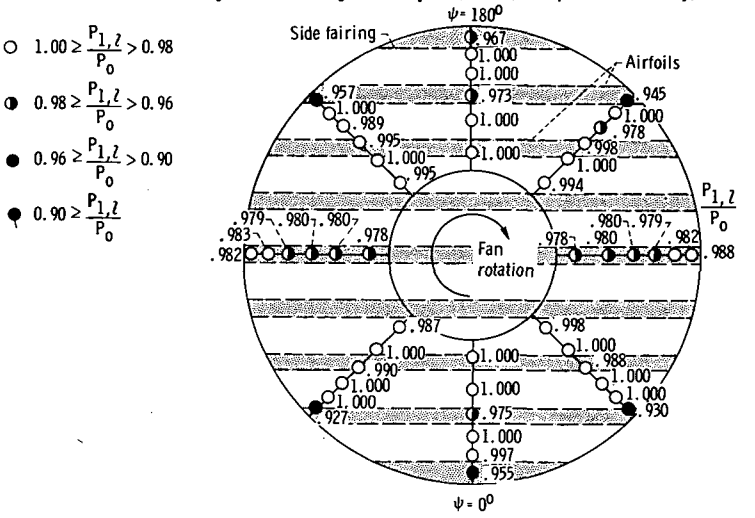

(b) Data point B; incidence angle, 30^0; corrected fan speed, 36 030 rpm; grid throat average Mach number, 0.559; total pressure recovery, 0.986.

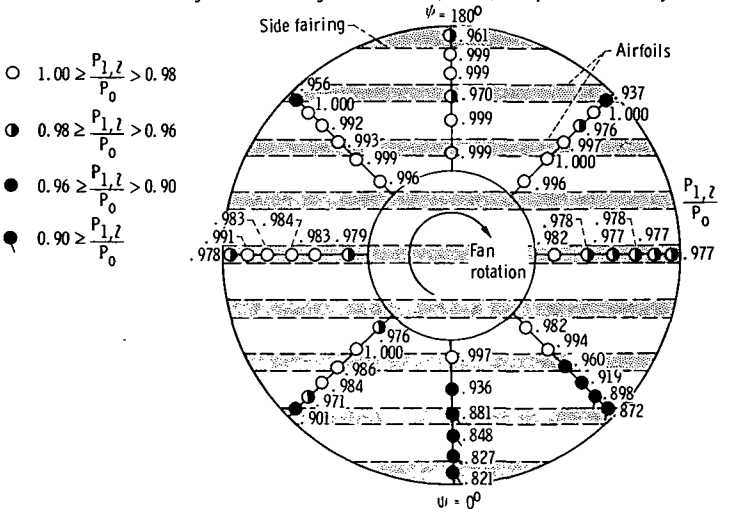

(c) Data point C; incidence angle, 40^0; corrected fan speed, 35 770 rpm; grid throat average Mach number, 0.541; total pressure recovery, 0.964.

Figure 4. - Total pressure distribution at rake measuring plane. Translating grid inlet in unchoked geometry, free-stream velocity, 45 meters per second.

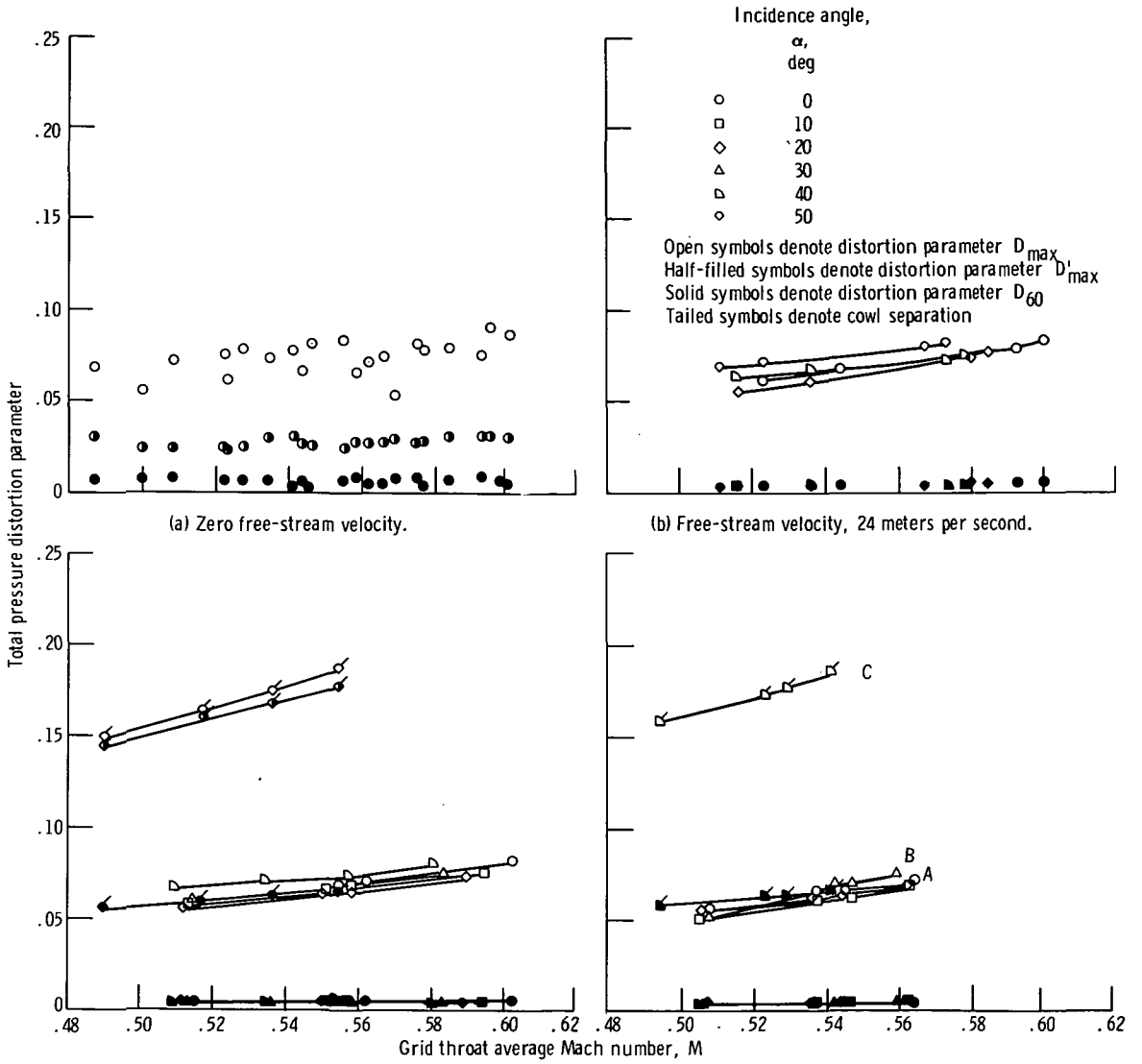

(a) Zero free-stream velocity.

(b) Free-stream velocity, 24 meters per second.

(c) Free-stream velocity, 32 meters per second.

(d) Free-stream velocity, 45 meters per second.

Figure 5. - Total pressure distortion generated by translating grid inlet in unchoked geometry.

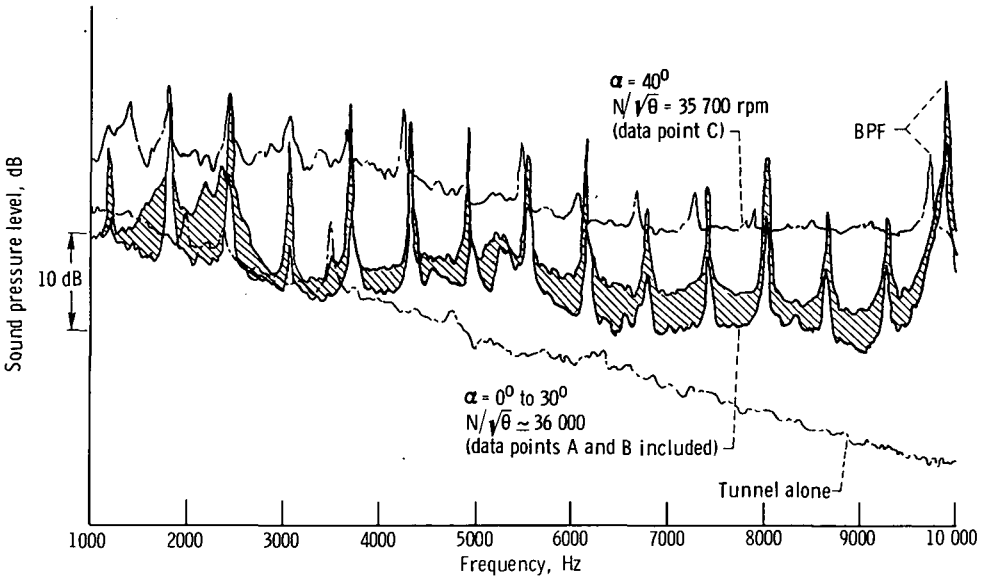

Figure 6. - Effect of incidence angle on noise generation. Translating grid inlet in unchoked geometry. Free-stream velocity, 45 meters per second; bandwidth, 20 hertz; 6-second sample.

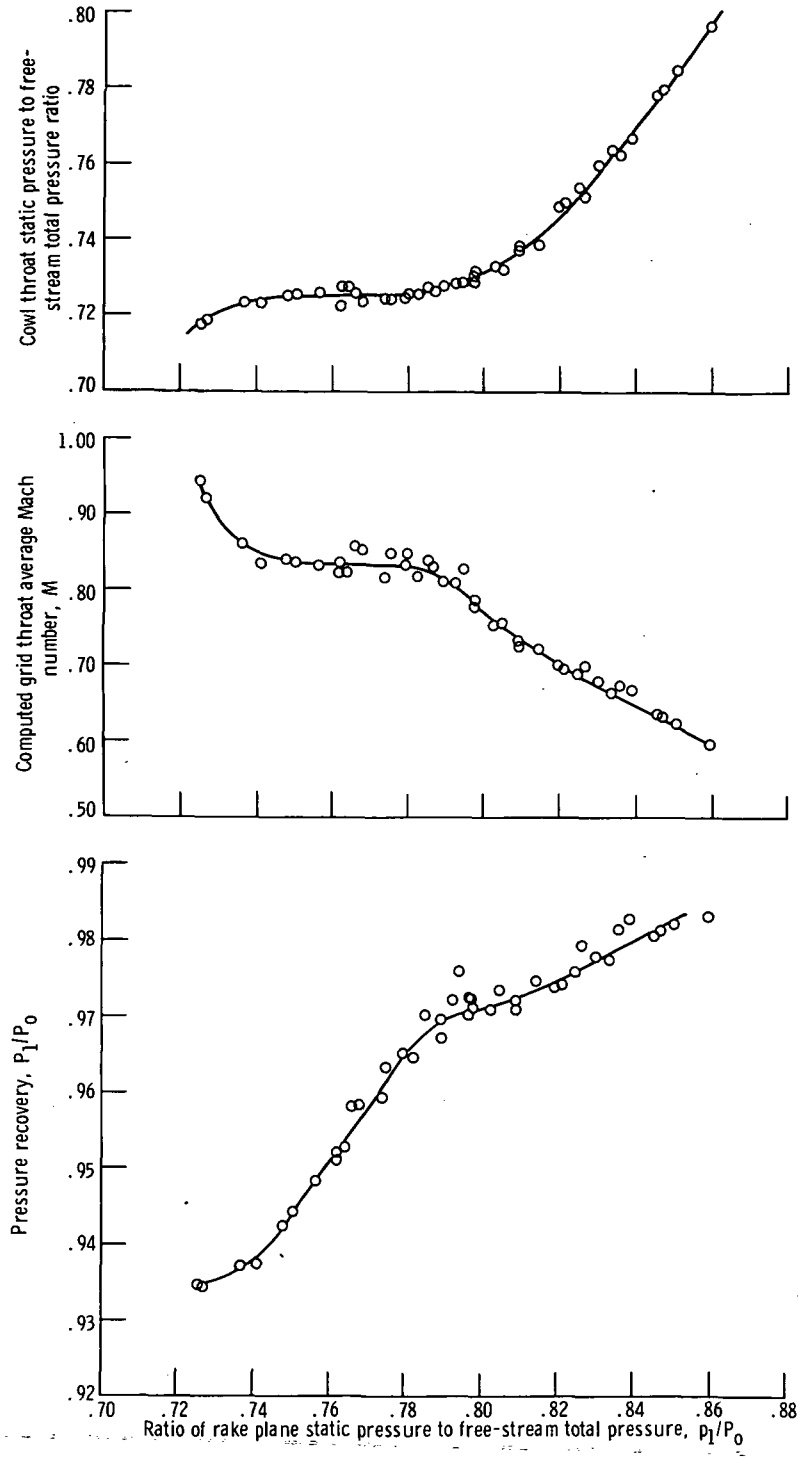

(a) Zero free-stream velocity.

Figure 7. - Average throat Mach number and inlet total pressure recovery of translating grid inlet in choked geometry.

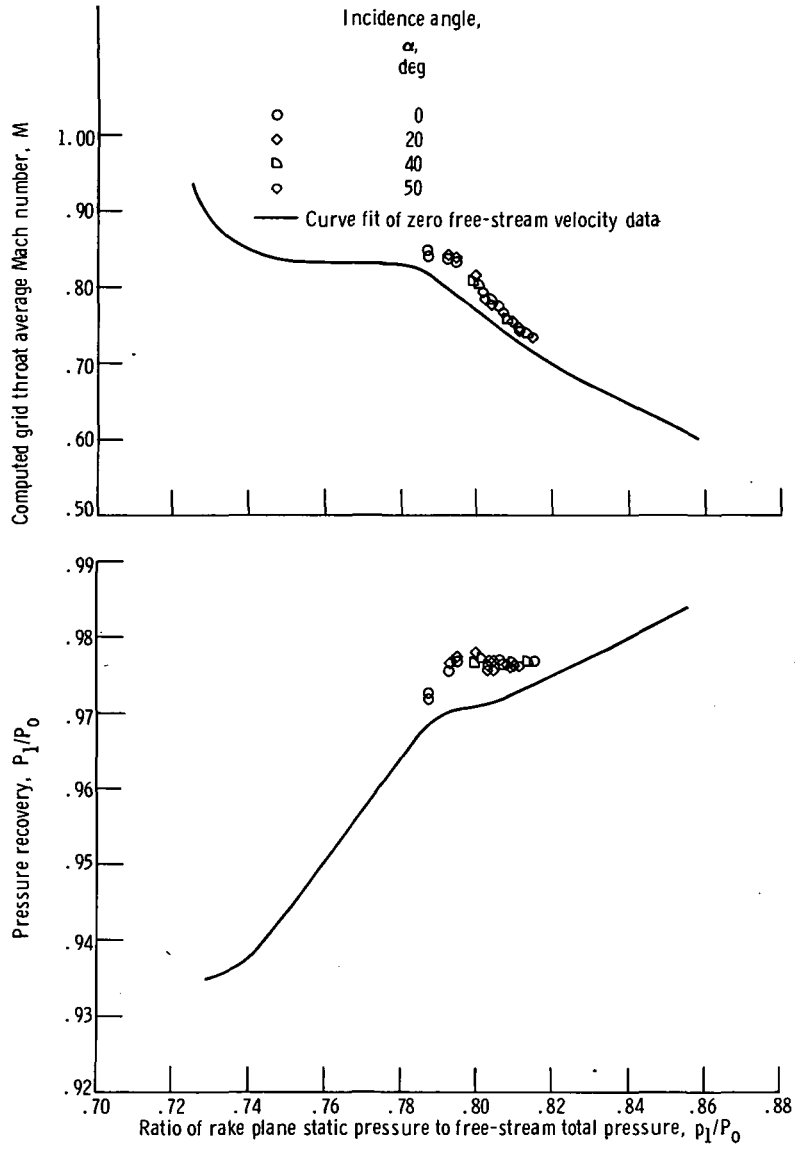

(b) Free-stream velocity, 24 meters per second.

Figure 7. - Continued.

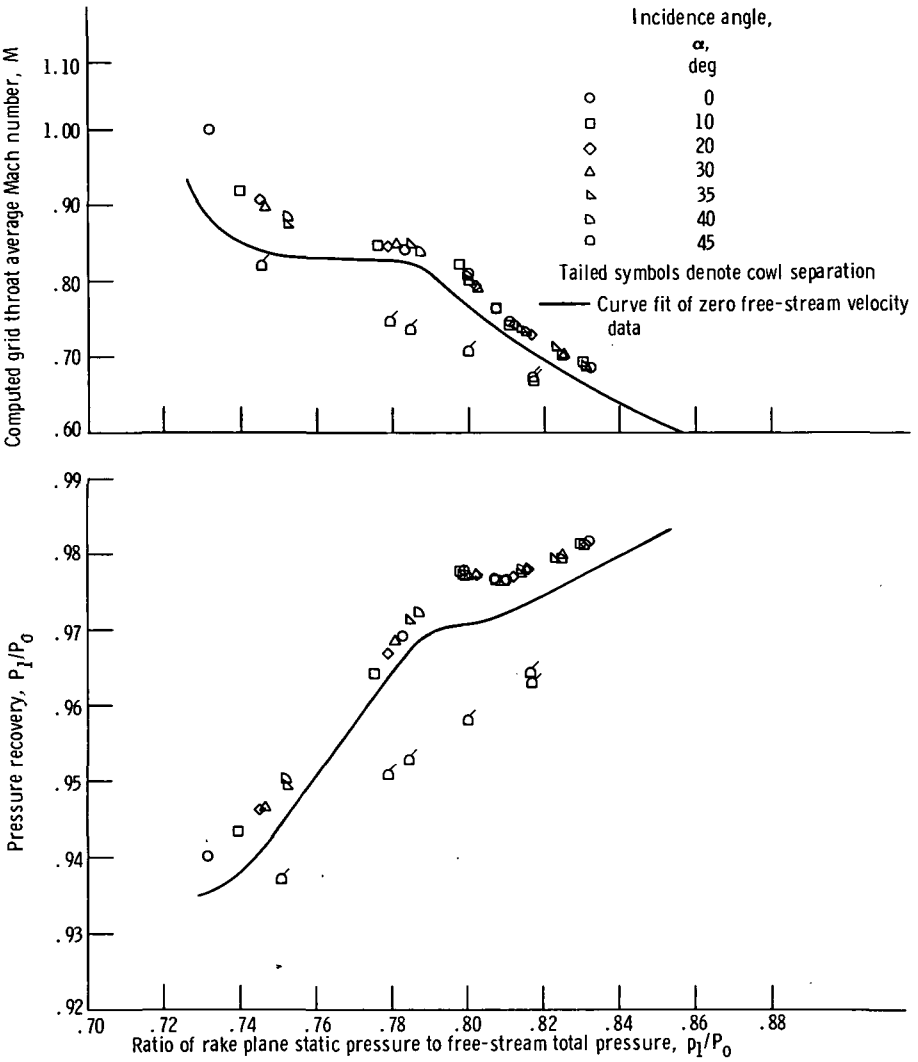

(c) Free-stream velocity, 32 meters per second.

Figure 7. - Continued.

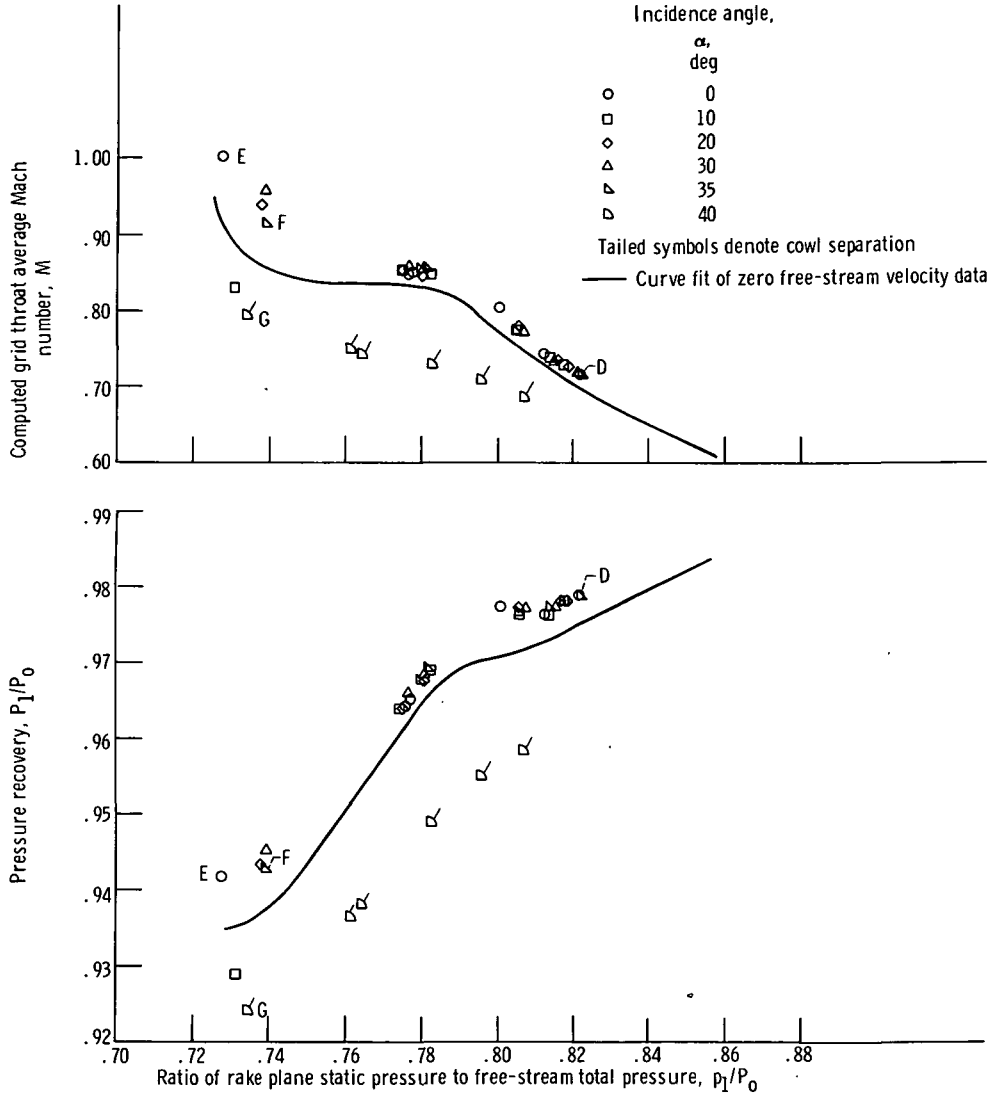

(d) Free-stream velocity, 45 meters per second.

Figure 7. - Concluded.

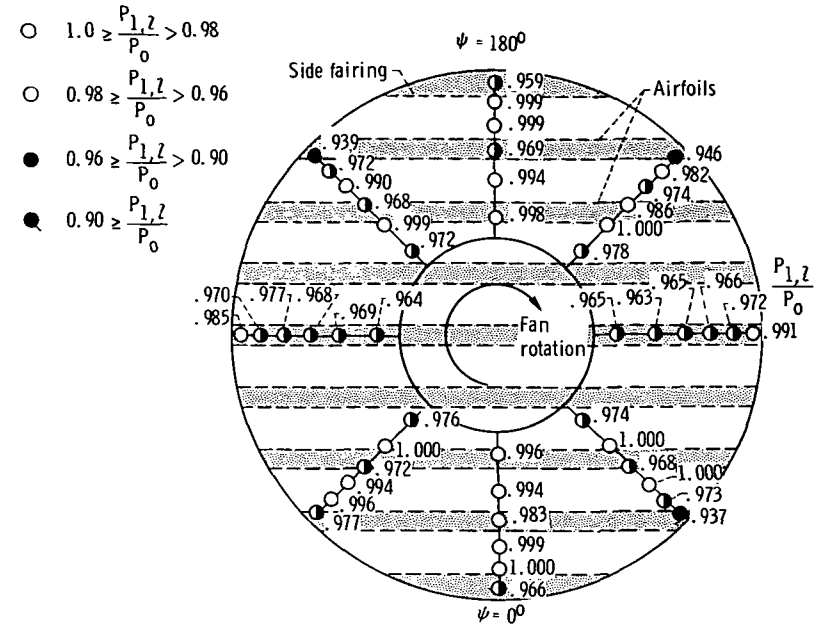

(a) Data point D; incidence angle, 0^0; corrected fan speed, 31 430 rpm; p_1/P_0, 0.822; total pressure recovery, 0.979.

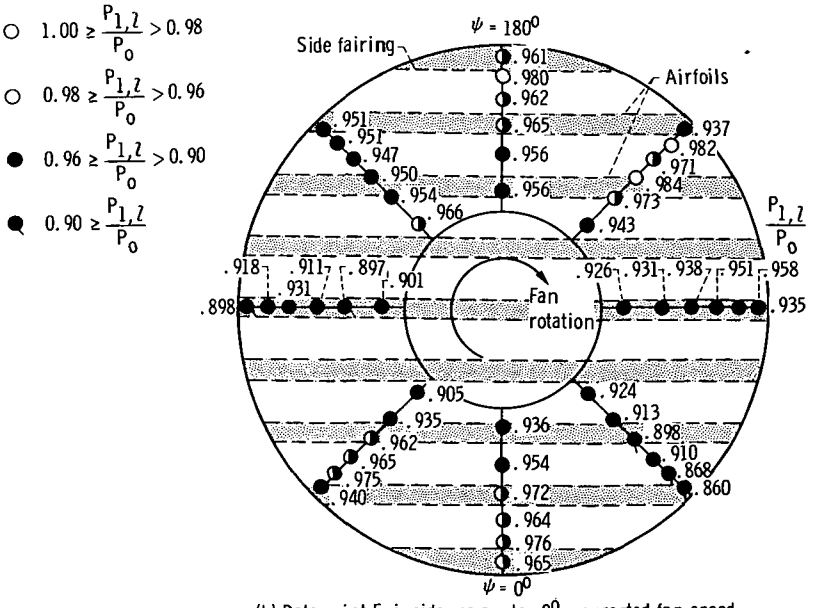

(b) Data point E; incidence angle, 0^0; corrected fan speed, 36 280 rpm; p_1/P_0, 0.728; total pressure recovery, 0.942.

Figure 8. - Total pressure distribution at rake measuring plane. Translating grid inlet in choked geometry. Free-stream velocity; 45 meters per second.

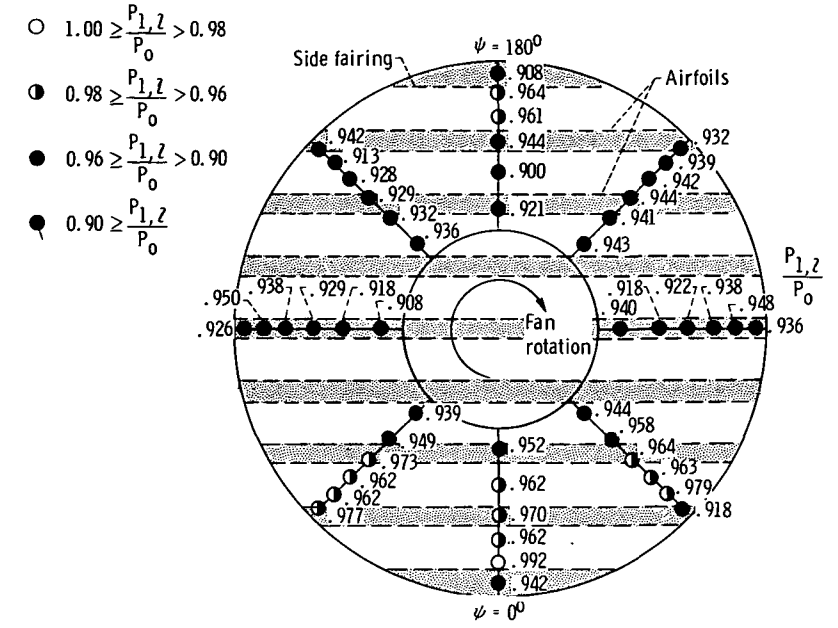

(c) Data point F; incidence angle, 35^0; corrected fan speed, 36 590 rpm; p_1/P_0, 0.739; total pressure recovery, 0.943.

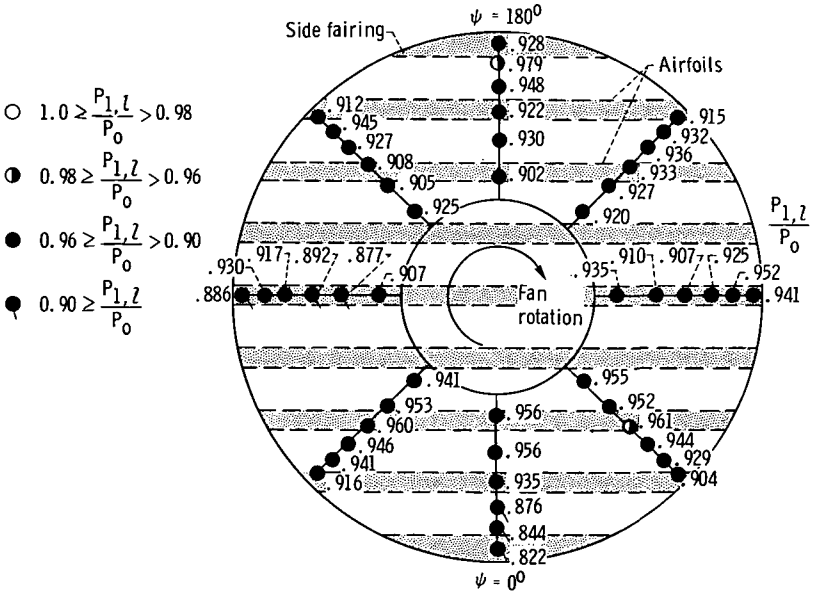

(d) Data point G; incidence angle, 40^0; corrected fan speed, 36 820 rpm; p_1/P_0, 0.734; total pressure recovery, 0.924.

Figure 8. - Concluded.

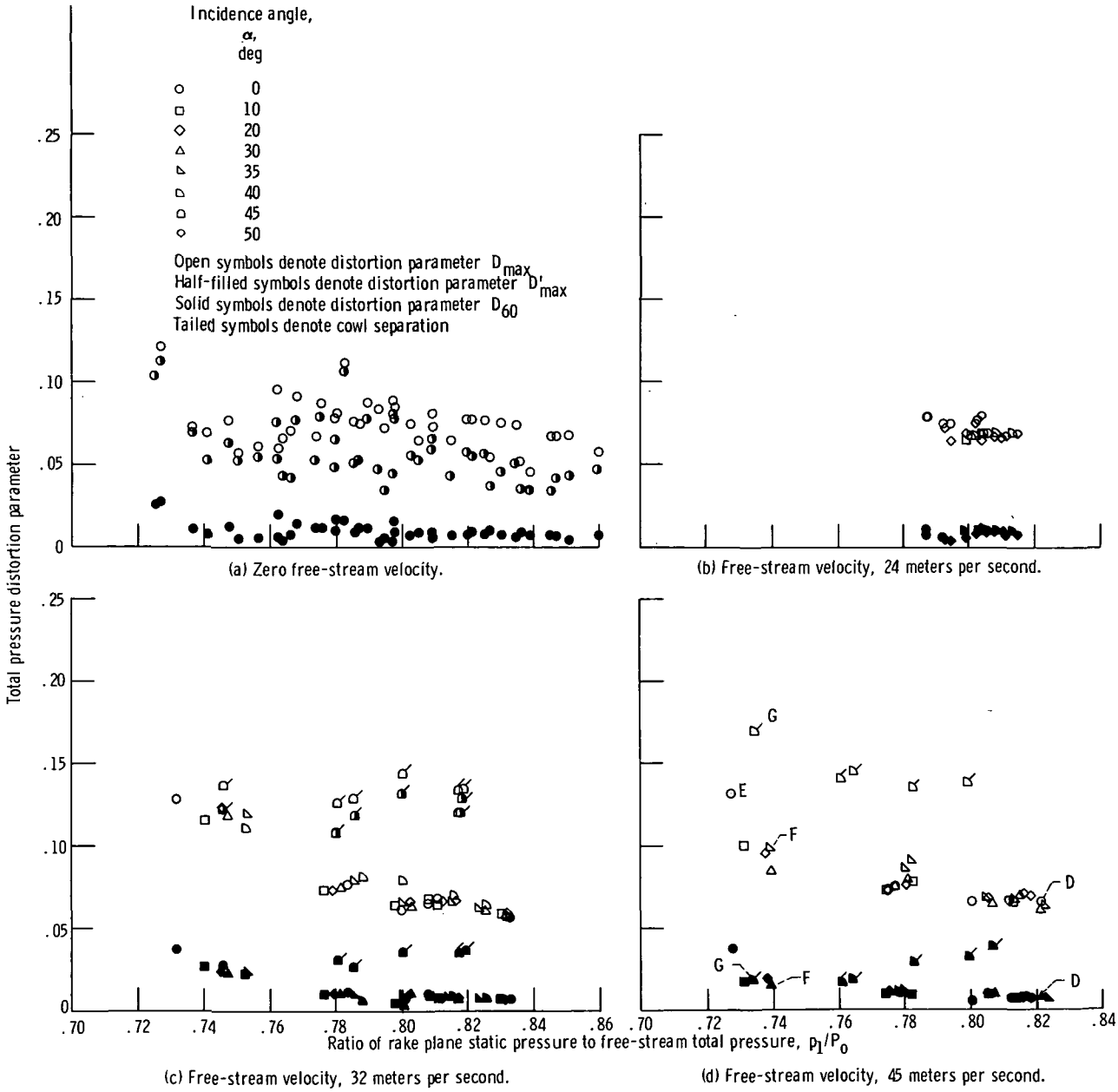

(a) Zero free-stream velocity.

(b) Free-stream velocity, 24 meters per second.

(c) Free-stream velocity, 32 meters per second.

(d) Free-stream velocity, 45 meters per second.

Figure 9. - Total pressure distortion generated by translating grid inlet in choked geometry.

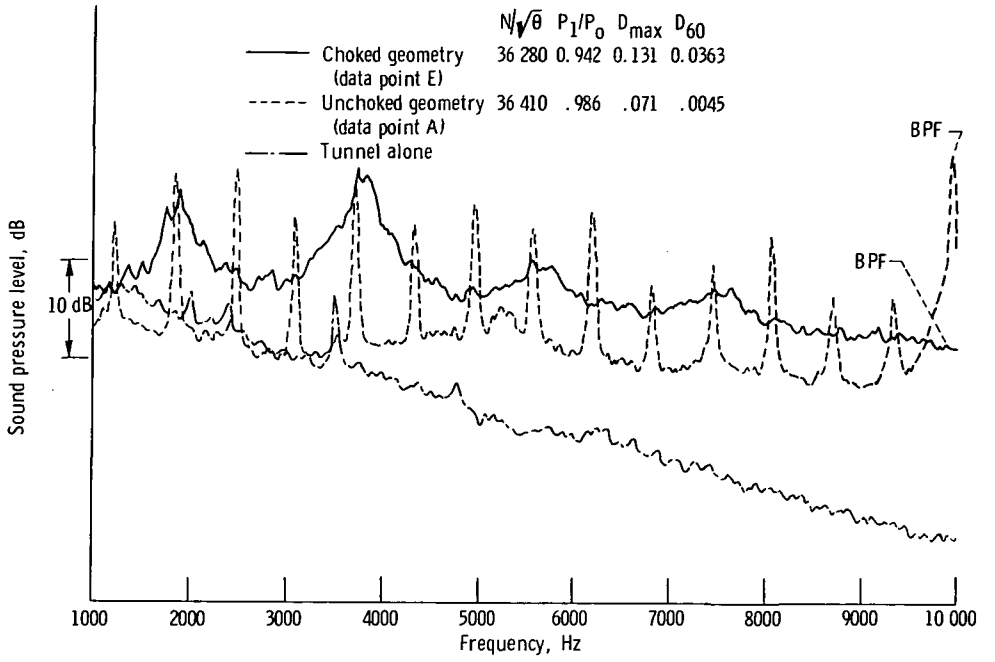

Figure 10. - Comparison of narrow band noise spectra for translating grid inlet operating in choked and unchoked geometries. Free-stream velocity, 45 meters per second; incidence angle, 0°; bandwidth, 20 hertz; 6-second sample.

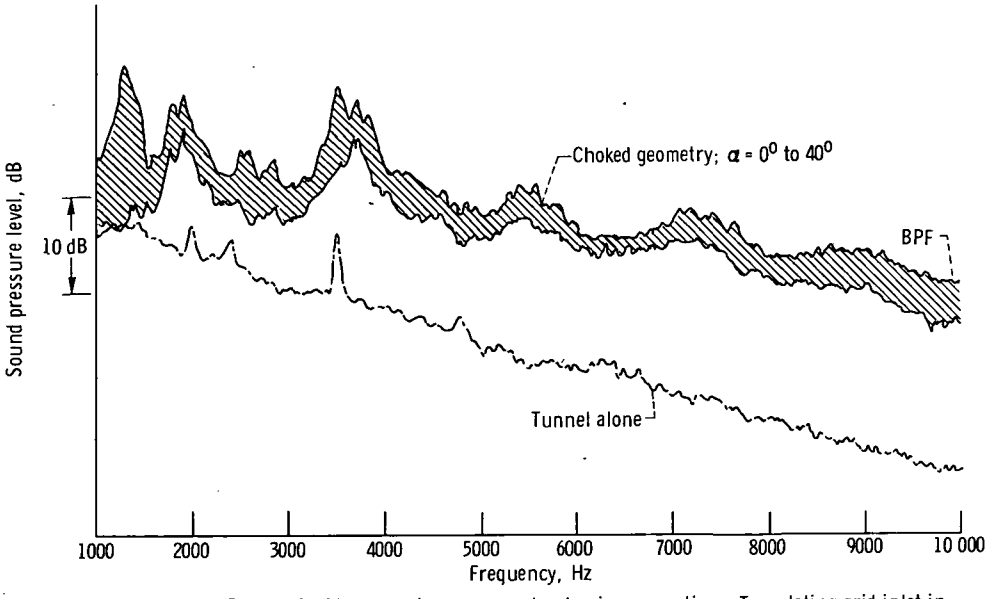

Figure 11. - Effect of incidence angle on narrow band noise generation. Translating grid inlet in choked geometry, free-stream velocity, 45 meters per second; average corrected fan speed, 36 450 rpm; bandwidth, 20 hertz, 6-second sample.

"The aeronautical and space activities of the United States shall be conducted so as to contribute . . . to the expansion of human knowledge of phenomena in the atmosphere and space. The Administration shall provide for the widest practicable and appropriate dissemination of information concerning its activities and the results thereof."

—NATIONAL AERONAUTICS AND SPACE ACT OF 1958

NASA SCIENTIFIC AND TECHNICAL PUBLICATIONS

TECHNICAL REPORTS: Scientific and technical information considered important, complete, and a lasting contribution to existing knowledge.

TECHNICAL NOTES: Information less broad in scope but nevertheless of importance as a contribution to existing knowledge.

TECHNICAL MEMORANDUMS: Information receiving limited distribution because of preliminary data, security classification, or other reasons. Also includes conference proceedings with either limited or unlimited distribution.

CONTRACTOR REPORTS: Scientific and technical information generated under a NASA contract or grant and considered an important contribution to existing knowledge.

TECHNICAL TRANSLATIONS: Information published in a foreign language considered to merit NASA distribution in English.

SPECIAL PUBLICATIONS: Information derived from or of value to NASA activities. Publications include final reports of major projects, monographs, data compilations, handbooks, sourcebooks, and special bibliographies.

TECHNOLOGY UTILIZATION PUBLICATIONS: Information on technology used by NASA that may be of particular interest in commercial and other non-aerospace applications. Publications include Tech Briefs, Technology Utilization Reports and Technology Surveys.

Details on the availability of these publications may be obtained from:

SCIENTIFIC AND TECHNICAL INFORMATION OFFICE

NATIONAL AERONAUTICS AND SPACE ADMINISTRATION

Washington, D.C. 20546